JBC RESEARCH ARTICLE

Molecular insight into regioselectivity of transfructosylation catalyzed by GH68 levansucrase and β-fructofuranosidase

Received for publication, December 1, 2020, and in revised form, February 2, 2021 Published, Papers in Press, February 8, 2021,
https://doi.org/10.1016/j.jbc.2021.100398

Masayuki Okuyama*,‡, Ryo Serizawa‡, Masanari Tanuma, Asako Kikuchi, Juri Sadahiro, Takayoshi Tagami, Weeranuch Lang, and Atsuo Kimura*

From the Research Faculty of Agriculture, Hokkaido University, Sapporo, Japan

Edited by Gerald Hart

Glycoside hydrolase family 68 (GH68) enzymes catalyze β-fructosyltransfer from sucrose to another sucrose, the so-called transfructosylation. Although regioselectivity of transfructosylation is divergent in GH68 enzymes, there is insufficient information available on the structural factor(s) involved in the selectivity. Here, we found two GH68 enzymes, β-fructofuranosidase (FFZ*m*) and levansucrase (LSZ*m*), encoded tandemly in the genome of *Zymomonas mobilis*, displayed different selectivity: FFZ*m* catalyzed the β-(2→1)-transfructosylation (1-TF), whereas LSZ*m* did both of 1-TF and β-(2→6)-transfructosylation (6-TF). We identified His79^{FFZm} and Ala343^{FFZm} and their corresponding Asn84^{LSZm} and Ser345^{LSZm} respectively as the structural factors for those regioselectivities. LSZ*m* with the respective substitution of FFZ*m*-type His and Ala for its Asn84^{LSZm} and Ser345^{LSZm} (N84H/S345A-LSZ*m*) lost 6-TF and enhanced 1-TF. Conversely, the LSZ*m*-type replacement of His79^{FFZm} and Ala343^{FFZm} in FFZ*m* (H79N/A343S-FFZ*m*) almost lost 1-TF and acquired 6-TF. H79N/A343S-FFZ*m* exhibited the selectivity like LSZ*m* but did not produce the β-(2→6)-fructoside-linked levan and/or long levanooligosaccharides that LSZ*m* did. We assumed Phe189^{LSZm} to be a responsible residue for the elongation of levan chain in LSZ*m* and mutated the corresponding Leu187^{FFZm} in FFZ*m* to Phe. An H79N/L187F/A343S-FFZ*m* produced a higher quantity of long levanooligosaccharides than H79N/A343S-FFZ*m* (or H79N-FFZ*m*), although without levan formation, suggesting that LSZ*m* has another structural factor for levan production. We also found that FFZ*m* generated a sucrose analog, β-D-fructofuranosyl α-D-mannopyranoside, by β-fructosyltransfer to D-mannose and regarded His79^{FFZm} and Ala343^{FFZm} as key residues for this acceptor specificity. In summary, this study provides insight into the structural factors of regioselectivity and acceptor specificity in transfructosylation of GH68 enzymes.

The so-called fructooligosaccharides (FOSs) are structurally divided into two types: the reducing FOSs and the nonreducing FOSs. The former is composed of only fructose units with reducing power, whereas the latter has the former conformation blocked by a glucose unit at its reducing fructosyl residue, thereby meaning "glucosides" (or "fructoside" for disaccharide). Natural nonreducing FOSs are mainly categorized into inulooligosaccharide (INO; whose long saccharide is an inulin with less than around sixty β-(2→1)-linked fructosyl units) and levanooligosaccharide (LVO; whose polysaccharide is a levan linked by β-(2→6)-fructosyl units). Also, natural reducing FOSs are present by cleaving a terminal Glc-Fru unit (sucrose unit) of INO or LVO with α-glucosidase and acidic condition. These natural FOSs are originally regarded to be responsible for energy storage in plants. Other possible functions, including their contribution to the tolerance against drought and freezing, are also proposed in plants and microbes (1). Moreover, their associated health benefits also receive considerable attention, such as the selective stimulation of the growth and/or the activity of beneficial intestinal bacteria, contributing to the increase of the absorption of several minerals as well as the lowering of the cholesterol levels (2–4).

Figure 1 depicts the structures of INO (*e.g.*, 1-kestose and nystose), LVO (*e.g.*, 6-kestose), levan, and neokestose [*e.g.*, β-fructosyl-(2→6)-glucosyl fructoside]. These nonreducing FOSs and levan are produced from sucrose with the aid of fructosyltransferring enzymes. Syntheses of INOs and inulin in plants are initiated by sucrose:sucrose 1-fructosyltransferase, resulting in 1-kestose. Subsequently, 1-kestose is further elongated by the action of fructan:fructan 1-fructosyltransferase. In microorganisms, the inulosucrase is responsible for the inulin synthesis. β-Fructofuranosidase (FF) is often used for the *in vitro* synthesis of INO, including commercially available INO, such as the 1-kestose and the nystose, which are produced by fungal FF (3). On the other hand, LVO and levan are well known to be produced by microbial levansucrase (LS). Plants, including timothy (*Phleum pratense*), orchard grass (*Dactylis glomerate*), and big bluegrass (*Poa secunda*), accumulate simple linear levan, of which timothy is identified to be synthesized with sucrose:fructan 6-fructosyltransferase (5, 6). 6-Kestose is also demonstrated to be efficiently formed by Microbial FF from *Schwanniomyces occidentalis* (7, 8). Furthermore, neokestose, neonystose, and the same type of long oligosaccharides are synthesized by FF in *Xanthophyllomyces dendrorhous* (9), a mutated FF of *S. occidentalis* (10), and a plant fructan:fructan 6^{G}-fructosyltransferase (11, 12), in which the term for the produced saccharides (*e.g.*, neokestose and neonystose) may become "neolevanooligosaccharides."

‡ These authors contributed equally to this work.
* For correspondence: Masayuki Okuyama, okuyama@abs.agr.hokudai.ac.jp; Atsuo Kimura, kimura@abs.agr.hokudai.ac.jp.

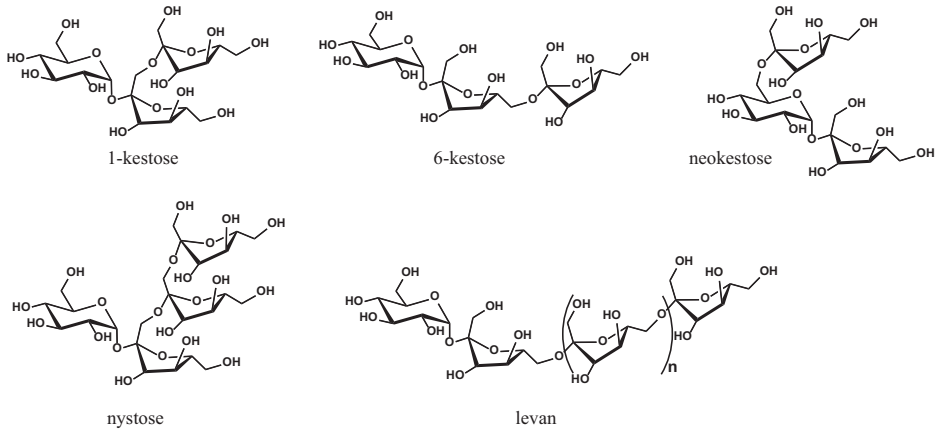

Figure 1. Structure of INO (1-kestose and nystose), LVO (6-kestose), levan, and neokestose.

Fructosyl-linkage hydrolyzing and transferring enzymes acting on sucrose are classified as members of the glycoside hydrolase family (GH) 32 or 68 (13). Among them, plant-derived enzymes and fungal FF generally belong to GH32, whereas the inulosucrase, LS, and bacterial FF are classified as GH68. GH32, and 68 proteins have a 5-bladed β-propeller fold as a catalytic domain, grouped into clan GH-J. The enzymes in this clan are known to show a catalytic double displacement mechanism with two carboxy groups, a catalytic nucleophile, and a general acid/base, for hydrolysis and/or transfructosylation. During the synthesis of inulin and levan, the transfructosylation occurs successively.

Bacterial LS, especially LS from Gram-positive *Bacillus* spp. (LS*Bspp*), is one of the most characterized GH68 enzymes (14–16). The molecular weight of the levan produced by these LS*Bspp*s, reaching 3×10^6, can be controlled by the reaction conditions and the mutagenesis of the enzyme. The protein engineering works and other results are well reviewed by Oritiz-Soto *et al.* (17). There are different types of LSs derived from Gram-negative bacteria, a *Gluconacetobacter diazotrophicus* LS (LS*Gd*) and an *Erwinia amylovora* LS (LS*Ea*), which synthesize a low amount of levan with the low molecular weight (18–20). Interestingly, a certain amount of INO (1-kestose and nystose) are also produced by these enzymes (18, 20), which is assumed to be associated with the low levan synthesis, although the detail mechanism is still obscure.

Gram-negative *Zymomonas mobilis* is known to grow on sucrose, glucose, and fructose as a carbon source. Therefore, it is possible that the enzymes associated with sucrose degradation of this bacterium have undergone its own molecular evolution under the limitation of having to use sucrose as a carbon source. *Z. mobilis* has two GH68 enzyme genes with ZZ6_0874 and ZZ6_0875 locus tags, which are positioned side by side in the chromosome, as if one of them was formed by a tandem gene duplication. Gene duplication has been of long-standing interest in the evolution as once a gene has duplicated, a novel function may be acquired by one of the copies (21). In fact, the functional evolution has occurred in these two GH68 proteins: ZZ6_0874 and ZZ6_0875 encode FF and LS (22–24), which hereafter will be referred to as FF*Zm* and LS*Zm*, respectively. The motivation for this study is to compare the structure and function of these enzymes that have undergone molecular evolution while relatively retaining sequence identity and to clarify the structural factors that distinguish the reaction specificity of two enzymes that act on sucrose. Relationship between the structure of LS*Zm* and its levan synthesis has been well-studied (25–27), while limited enzymatic study has been done on FF*Zm*, which might be due to the lack of clear difference in regard of the molecular mechanisms between the two GH68 enzymes in *Z. mobilis*. In this study, we found a distinction in regioselectivity of the FF*Zm*- and LS*Zm*-catalyzed transfructosylation as well as identified the structural factors responsible for the regioselectivity by mutation works. Until now, no studies have been performed to our knowledge on the regulation of the regioselectivity of GH68 enzymes. Our mutation works also enabled to learn one of important residues to elongate LVO chain. The FF*Zm* was found to generate β-D-fructofuranosyl α-D-mannopyranoside (Fru-Man; a sucrose analog) with a good yield, which was firstly produced by *Bacillus subtilis* LS (LS*Bc*) (28), although in not high-yield formation.

Results and discussion

*Characterization and initial transfructosylation of the LS*Zm *and FF*Zm

Wild-type LS*Zm* and FF*Zm* had the specific activities of 247 and 1620 U mg^{-1}, respectively (Table 1). The pH optimum for both enzymes was at pH 5.0, and the pH stability was between pH 4.2 and 5.5 after treatment at 4 °C for 24 h, as well as the thermal stability was up to 45 °C after a 15 min incubation. Although the initial velocity can be measured at 45 °C, the following transfructosylation experiments were carried out at 35 °C, where the activities were maintained even after prolonged reaction.

The LS*Zm*- and FF*Zm*-catalyzed initial 10 min reaction was analyzed using various sucrose concentrations ([sucrose]) (Fig. 2, *A* and *B*, respectively), in which the formed carbohydrates were measured with high-performance anion-exchange chromatography with pulsed amperometric detection (HPAEC-PAD). The initial products were glucose, fructose,

Table 1
Properties of FF*Zm*, LS*Zm*, and their variants

Enzyme	Specific activity (U mg^{-1})	Optimum pH	pH-stability[a]	Thermal stability (°C)[b]
FF*Zm*				
Wild type	1620	5.0	4.2–6.0	<45
H79N-FF*Zm*	502	5.0	4.1–6.0	<40
A343S-FF*Zm*	380	5.0	4.1–6.0	<45
H79N/A343S-FF*Zm*	274	5.0	4.1–6.0	<45
H79N/L187F/A343S-FF*Zm*	350	5.0	4.1–6.0	<40
LS*Zm*				
Wild type	247	5.0	4.1–5.5	<45
N84H-LS*Zm*	480	5.5	3.7–5.5	<60
S345A-LS*Zm*	800	5.0	3.7–5.0	<60
N84H/S345A-LS*Zm*	440	5.5	3.7–5.5	<60

[a]pH stability or [b]thermal stability shows the range to maintain the residual activity of more than 90% [a] after treating with various pH at 4 °C for 24 h or [b] after incubating at various temperatures for 15 min, respectively.

1-kestose, and 6-kestose, at which the hydrolysis generates glucose and fructose from sucrose and water as well as the transfructosylation forms trisaccharide (1-kestose or 6-kestose) and glucose from two sucrose molecules. Therefore, the initial reactions of both enzymes follow the scheme of Figure 2*C*, similarly to many glycosylases (28). Transfructosylation products were different in LS*Zm* and FF*Zm*, where 6-kestose and 1-kestose were synthesized by the former (Fig. 2*A*), while 1-kestose with a trace amount of 6-kestose was synthesized by the latter (Fig. 2*B*). 1-Kestose (or 6-kestose) is produced from two-substrate reaction using two sucrose molecules as noted above, at which a fructosyl residue of donor sucrose is transferred to an acceptor sucrose to form the β-(2→1)-fructoside linkage [or β-(2→6)-fructoside linkage]. The formation velocities of the transfructosylation products, 6-kestose ($v_{6\text{-kestose}}$ $[E]_0^{-1}$; abbreviated as $v_{6\text{-Kes}}$) and 1-kestose ($v_{1\text{-kestose}}$ $[E]_0^{-1}$; $v_{1\text{-Kes}}$), increased with an increase of [sucrose] (Fig. 2, *A* and *B*). In the range of [sucrose] up to 300 mM, the formation velocities of glucose ($v_{glucose}$ $[E]_0^{-1}$; v_{Glc}) and fructose ($v_{fructose}$ $[E]_0^{-1}$; v_{Fru}) increased with showing almost equal amounts (Fig. 2, *A* and *B*), meaning that the main reaction is a hydrolysis. Moreover, as a [sucrose] increased, v_{Glc} and v_{Fru} decreased (especially v_{Fru}), meaning that the hydrolysis reduces and the transfructosylation increases. According to the scheme that is followed by the LS*Zm* and the FF*Zm* (Fig. 2*C*), the velocity of hydrolysis is reflected by v_{Fru}, and that of transfructosylation is indicated by $v_{6\text{-Kes}}$ and/or $v_{1\text{-Kes}}$. The v_{Glc} represents a sucrose degradation velocity, meaning the whole reaction velocities, *i.e.*, the sum of hydrolysis and transfructosylation. The decrease in v_{Fru} can be ascribed to the increase in transfructosylation at the high [sucrose]. On the other hand, the diminution in v_{Glc} indicates the substrate inhibition of enzyme reaction. There are two possibilities that can explain this inhibitory phenomenon. First, the accumulation of an E-F·F-G complex is assumed (Fig. 2*C*) (29, 30). The concentration of the E-F·F-G complex ([E-F·F-G]) increases with increasing [sucrose], eventually exceeding the limit of the ability to catalyze the fructosidic linkage formation, so that the accumulation of the E-F·F-G is expected to occur. Since the [E·F-G], [E-F], and [E-F·F-G] are in steady state, an increase in the [E-F·F-G] causes a decrease in the v_{Glc}. Secondly, a nonproductive binding that, for instance, the excess sucrose occupies the +1 and +2 subsites of the catalytic site, prevents the productive binding of the sucrose at −1 and +1 subsites (31). The occurrence of the nonproductive binding increases at a higher [sucrose]. We cannot identify the correct mechanism among the two possibilities [or more correct further candidate(s) might exist, if the above two possibilities are not accurate].

The proportion of the transfructosylation velocity in all reaction velocities, which can be estimated from the equation of $(v_{1\text{-kestose}} + v_{6\text{-kestoe}})/v_{glucose}$, was 0.52 in LS*Zm* and 0.34 in FF*Zm* using 1 M sucrose as substrate (Table 2). Yanase *et al.* (24) reported that the FF*Zm*, purified from the periplasmic fraction of *Z. mobilis*, exhibited no transfructosylation activity, in regard of which the detailed experimental conditions were missing. A certain reaction condition might be inadequate, suggesting that one factor is a less enough [sucrose].

Transfructosylation of LSZm and FFZm at late reaction stage

The LS*Zm*- and FF*Zm*-generating transfructosylation products from 1 M sucrose were analyzed at 1 h (Fig. 3). The wild-type LS*Zm* synthesized 6-kestose, 1-kestose, and neokestose (Fig. 3*A*). Neokestose, produced by β-(2→6)-transfructosylation (6-TF) of a fructose unit to the glucosyl residue of sucrose, was not detected during the initial reaction, implying a slower formation than that of the 6-kestose and 1-kestose. At 24 h, LS*Zm* formed several oligosaccharides (6-kestose, neokestose, and nystose) as well as some possible LVOs with high degree of polymerizations (DPs) (Fig. 3*B*). The long LVOs should have DPs at least 25 (inset of Fig. 3*B*), although their exact DPs could not be estimated due to unavailable standards. They might be the intermediates of low-molecular weight levan after the elongation with successive 6-TF. On the other hand, the FF*Zm* generated a sole trisaccharide of 1-kestose at 1 h (Fig. 3*C*). At 24 h, further trisaccharides of the 6-kestose, neokestose, and nystose were observed along with a small amount of the products above DP4 (Fig. 3*D*). In cases of both initial and late reaction stages, FF*Zm* and LS*Zm* show different regioselectivity in the transfructosylation process (Figs. 2 and 3), at which the former mainly catalyzes β-(2→1)-transfructosylation (1-TF), whereas the latter does both of 1-TF and 6-TF.

Table 2
Reaction velocities of FFZ*m*, LSZ*m*, and their variants against 1 M sucrose

Enzyme	$v_{glucose}$ $[E]_0^{-1}$ (s^{-1})	$v_{fructose}$ $[E]_0^{-1}$ (s^{-1})	$v_{1\text{-kestose}}$ $[E]_0^{-1}$ (s^{-1})	$v_{6\text{-kestose}}$ $[E]_0^{-1}$ (s^{-1})	Transfructosylation ratio[a]	$v_{6\text{-kestose}}/(v_{1\text{-kestose}} + v_{6\text{-kestose}})$ (%)
FFZ*m*						
Wild type	2980 ± 360	1960 ± 310	1150 ± 160	45 ± 4	0.34	3.8
H79N-FFZ*m*	1500 ± 130	1200 ± 42	65 ± 8	48 ± 9	0.20	42
A343S-FFZ*m*	200 ± 9	160 ± 6	12 ± 1	4.8 ± 0.3	0.20	29
H79 N/A343S-FFZ*m*	600 ± 29	505 ± 52	1.7 ± 0.6	51 ± 5	0.16	97
H79N/L187F/A343S-FFZ*m*	920 ± 23	600 ± 35	12 ±0.9	190 ± 15	0.35	94
LSZ*m*						
Wild type	1820 ± 216	870± 193	216 ± 13	370 ± 84	0.52	63
N84H-LSZ*m*	790 ± 59	330 ± 23	420 ± 69	3.0 ± 0.1	0.58	7
S345A-LSZ*m*	1400 ± 66	480 ± 63	360 ± 8	52 ± 5	0.66	13
N84H/S345A-LSZ*m*	1600 ± 120	500 ± 70	1100 ± 70	1.5 ± 0.2	0.69	0.14

[a] Transfructosylation ratio was calculated from the equation of $(v_{1\text{-kestose}} + v_{6\text{-kestose}}) / v_{glucose}$, indicative of the proportion of transfructosylation to whole reactions: *e.g.*, a transfructosylation ratio of 0.69 means 69% of transfructosylation and 31% of hydrolysis at 1M sucrose.

Prediction of residues responsible for regioselectivity of transfructosylation

As mentioned above, the regioselectivity of transfructosylation diverges at GH68 FFZ*m* and LSZ*m*, despite that their amino-acid sequences share the significantly high 61.5% identity and 72.0% similarity with only 5.1% gaps, leading us to unravel the structural factor(s) in connection with the regulation of regioselectivity distinction. However, the three-dimensional structures (3Ds) of these enzymes remain unresolved currently, and it is hard to identify the amino acid residues that are key to the differences in specificity. To visualize the 3Ds of amino acid residues at the active-site pocket of FFZ*m* and LSZ*m*, both enzymes were modeled (Fig. 4) using the 3D of LS*Ea* (32) as it had the most similarity to the amino-acid sequence of the 3D-known GH68 proteins. Pairwise alignments for the construction of model structures were created with Needleman–Wunsch algorithm using BLOSUM62 as the score matrix, and FFZ*m* and LSZ*m* showed 45.3% and 51.1% sequence identity with the template sequence, respectively. Comparative modeling was done in automodel mode of MODELLER. GA341 and zDOPE in the respective models were 1.0 and −0.88 (FFZ*m*) and 1.0 and −0.82 (LSZ*m*), indicating a reliable model. Besides, the 1-kestose and 6-kestose docked to FFZ*m* and LSZ*m* using AutoDock Vina (33), respectively. The docking scores were −7.5 (1-kestose to FFZ*m*) and −7.7 (6-kestose to LSZ*m*), respectively. The residues forming −1 and +1 subsites were well conserved, except for $His79^{FFZm}$ and $Ala343^{FFZm}$ (Fig. 4*A*), corresponding to $Asn84^{LSZm}$ and $Ser345^{LSZm}$, respectively (Fig. 4*B*). $His79^{FFZm}$ and $Asn84^{LSZm}$ are at an intervening loop between βIB and βIC of the blade I in 5-bladed β-propeller to participate in the +1 subsite. In the model structure, $His79^{FFZm}$ possibly forms a hydrogen bond with C6-OH of fructosyl residue on +1 subsite (Fig. 4*A*). $Asn84^{LSZm}$ likely forms two hydrogen bonds with C1-OH of fructosyl residues on the −1 and +1 subsites (Fig. 4*B*). Furthermore, both of $Ala343^{FFZm}$ and $Ser345^{LSZm}$, located on the βVA of the blade V, are in the inner part of active pocket, spatially situating close to Asp44 and Asp48 catalytic nucleophile residues, respectively (Fig. 4, *A* and *B*). We anticipated that these divergences were involved in regioselectivity difference, allowing to generate six mutated enzymes: H79N-FFZ*m*, A343S-FFZ*m*, H79N/A343S-FFZ*m*, N84H-LSZ*m*, S345A-LSZ*m*, and N84H/S345A-LSZ*m*.

Characterization of mutated enzymes

Identical procedures used for wild-type FFZ*m* and LSZ*m* were performed for characterizing their mutants (Table 1). The specific activities of FFZ*m* variants, measured using 50 mM sucrose, decreased to 31%–17%, whereas those of LSZ*m* derivatives increased to 176%–320%. Among these findings, the latter phenomena are of interest since generally mutated enzyme reduces specific activity. The original specific activity of wild-type FFZ*m* is greater than that of wild-type LSZ*m*, so that the other five mutants display similar values of 270–500 U mg^{-1}. S345A-LSZ*m* exhibits the highest value,

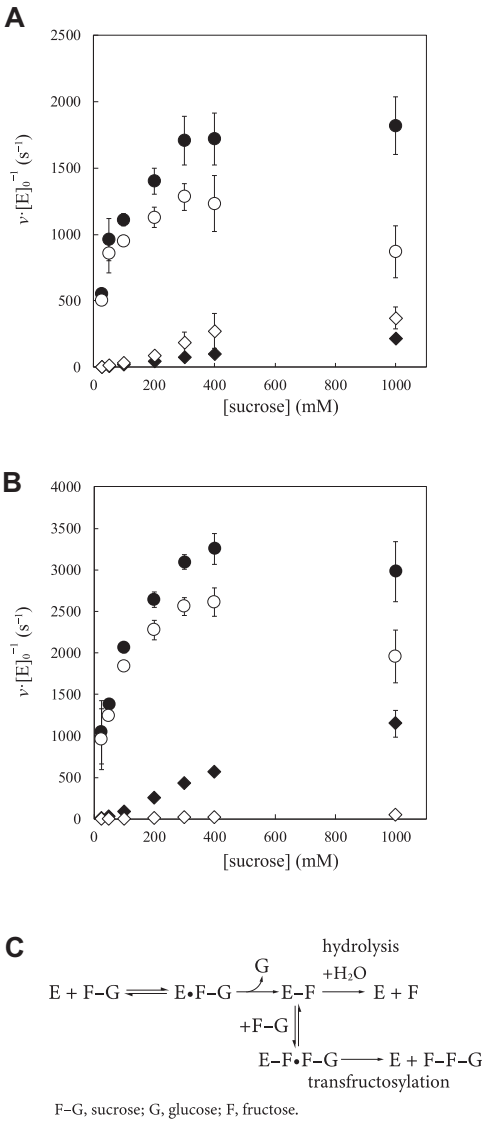

F–G, sucrose; G, glucose; F, fructose.

Figure 2. Initial reaction products of LS*Zm* and FF*Zm* from 1 M sucrose. *A* and *B*, plots of initial velocity *versus* [sucrose] for LS*Zm* (*A*) and FF*Zm* (*B*). Reactions were performed for 10 min at 35 °C and pH 5.0. HPAEC-PAD measured concentrations of saccharides: [fructose] (*open circle*), [glucose] (*closed circle*), [6-kestose] (*open diamond*), and [1-kestose] (*closed diamond*). Each experiment was repeated three times, and the mean was plotted (error bar, SD). *C*, reaction scheme. Free enzyme (E) binds to sucrose (F-G) to form the Michealis-complex (E·F-G), and release glucose (G) to form the second intermediate (E-F). The E-F either proceeds to hydrolysis to degrade into E and fructose (F) or to transfructosylation by accepting F–G to form the tertiary complex (E-F·F-G), which degrades into E and trisaccharide (F-F-G). F-F-G is 1-kestose or 6-kestose, depending on LS*Zm* or FF*Zm*.

800 U mg^{-1}, alternating its catalytic efficiency. Moreover, all mutants were similar to their parent enzymes in regard of their optimum pH and pH-stability range. The thermal stability of LS*Zm* variants is higher than that of their wild type, whereas FF*Zm* derivatives maintain the heat stability of their parent enzyme.

*Transfructosylation of LS*Zm *mutants*

The transfructosylation products of LS*Zm* mutants were identical to those of the wild type. The enzymes yielded 1-kestose and 6-kestose in the initial reaction mixture using 1 M sucrose as substrate. The initial v_{Glc}, v_{Fru}, $v_{1\text{-Kes}}$, and $v_{6\text{-Kes}}$ are summarized in Table 2. Two mutants, S345A-LS*Zm* and N84H/S345A-LS*Zm*, almost maintained the whole reaction velocities (v_{Glc}), whereas N84H-LS*Zm* decreased to 43% of the parent enzyme. All variants of LS*Zm* increased $v_{1\text{-Kes}}$ but decreased $v_{6\text{-Kes}}$. In comparison with wild type, $v_{1\text{-Kes}}$ increased to 170% (S345A-LS*Zm*) of parent value, 190% (N84H-LS*Zm*), and 510% (N84H/S345A-LS*Zm*), whereas $v_{6\text{-Kes}}$ did 14% (S345A-LS*Zm*), 0.8% (N84H-LS*Zm*), and 0.4% (N84H/S345A-LS*Zm*). An increase in the transfructosylation ratio of each mutant can be explained by the enhancement of $v_{1\text{-Kes}}$. Among the mutants, N84H/S345A-LS*Zm*, of which [$v_{6\text{-kestose}}/(v_{1\text{-kestose}} + v_{6\text{-kestose}})$] value is substantially small (0.14%), is found to be quite similar to FF*Zm* in regard of its trisaccharide production profile (Table 2).

Figure 3, *A* and *B* show the late reaction products of LS*Zm* mutants at 1 and 24 h, respectively. At 1 h, three variants displayed the lack or a decreased production of 6-kestose due to the reduction of $v_{6\text{-Kes}}$ at the initial reaction stage (Table 2), in which N84H-LS*Zm* maintained the less formation even at 24 h. While S345A-LS*Zm* still produced neokestose similarly to the wild type, N84H-LS*Zm* and N84H/S345A-LS*Zm* almost lost the formation of this trisaccharide. Besides, all mutations were observed to abolish the ability to generate large DP products (insets of Fig. 3*B*), probably coincident with the lowered capability to synthesize the β-(2→6)-fructosidic linkage. S345A-LS*Zm* could produce LVOs up to DP10 in trace amounts by maintaining a limited ability to catalyze the successive 6-TF. These results indicate that $Asn84^{LSZm}$ and $Ser345^{LSZm}$ are involved in the 6-TF specificity of LS*Zm*. The regioselectivity can be switched from LS*Zm*-type to FF*Zm*-type by the substitutions of $Asn84^{LSZm}$ and $Ser345^{LSZm}$ with FF*Zm*-type His and Ala, respectively.

*Transfructosylation of FF*Zm *mutants*

FF*Zm* variants (H79N-FF*Zm*, A343S-FF*Zm*, H79N/A343S-FF*Zm*), which synthesized the same initial products as wild type, decreased in every initial velocity [$v_{1\text{-Kes}}$, v_{Fru}, and v_{Glc} (total reaction velocity)]. The mutants showed a decreased transfructosylation ratio but an enhanced [$v_{6\text{-kestose}}/(v_{1\text{-kestose}} + v_{6\text{-kestose}})$] value (Table 2). These results are attributed to the substantial reduction in $v_{1\text{-Kes}}$. Even H79N-FF*Zm*, which showed the highest value in the mutants, decreased to 5.7% compared with that of the wild type. While $v_{6\text{-Kes}}$ decreased to 11% in A343S-FF*Zm*, it increased slightly in H79N-FF*Zm* and H79N/A343S-FF*Zm*. The H79N/A343S-FF*Zm*, of which $v_{1\text{-Kes}}$ decreased greatly, demonstrates the notable [$v_{6\text{-kestose}}/(v_{1\text{-kestose}} + v_{6\text{-kestose}})$] value (97%), and its regioselectivity almost completely changes from 1-TF to 6-TF.

The late reaction of FF*Zm* mutants at 1 and 24 h is shown in Figure 3, *C* and *D*, respectively. At 1 h, H79N-FF*Zm* and A343S-FF*Zm* synthesized both the 6-kestose and 1-kestose. H79N/A343S-FF*Zm* did 6-kestose as the almost sole transfrucosylation product similarly to initial reaction, although the synthesis of 6-kestose was not found in the wild type. At 24 h,

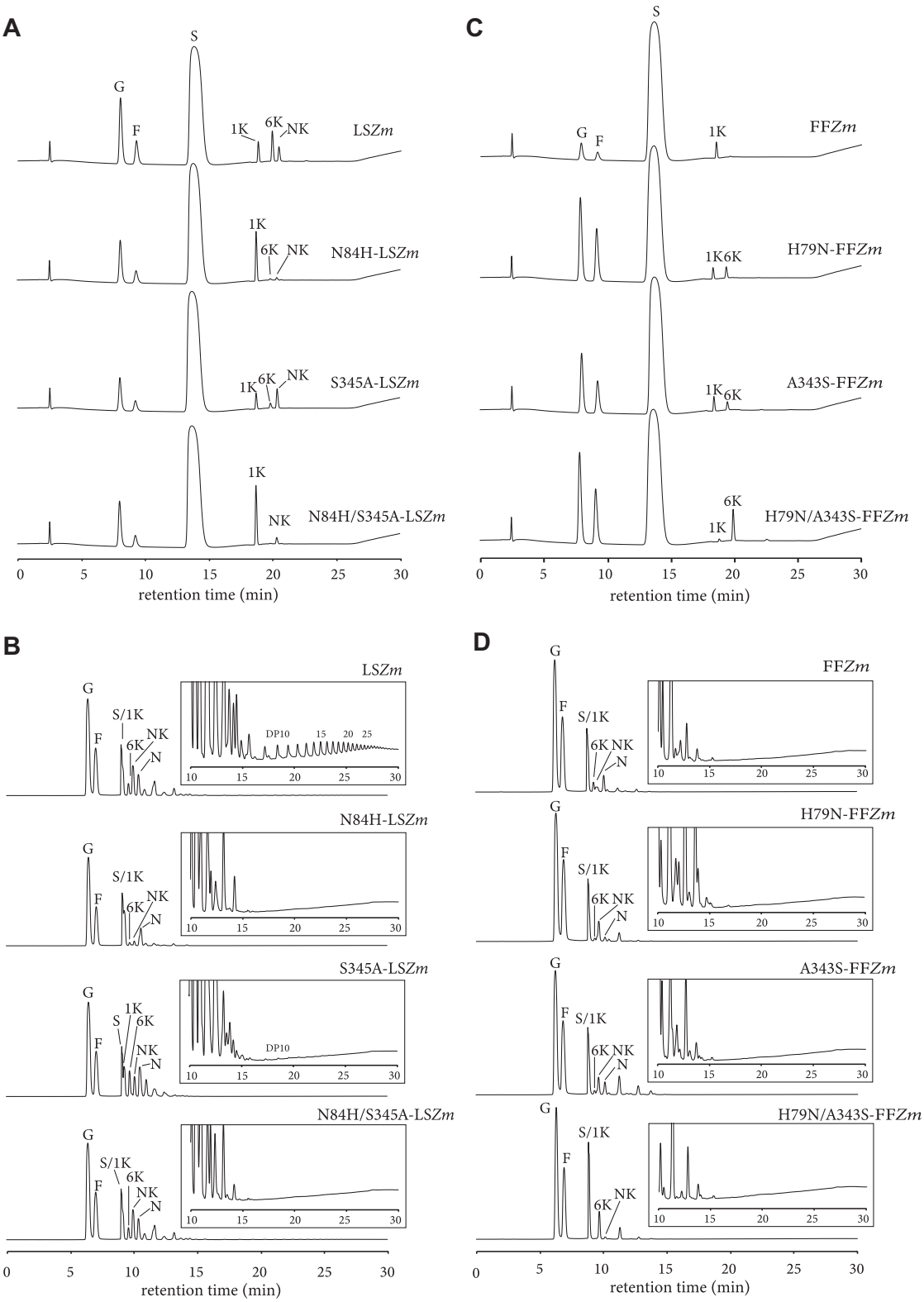

Figure 3. Products at the late reaction stages of LS*Zm*, FF*Zm*, and their variants from 1 M sucrose. *A* and *B*, LS*Zm* and its variants at 1 h (*A*) and 24 h (*B*). *C* and *D*, FF*Zm* and its variants at 1 h (*C*) and 24 h (*D*). *Insets* of *B* and *D* are the magnified figures to clearly display the long saccharides with a small amount. F, fructose; G, glucose; S, sucrose; N, nystose; NK, neokestose; 1K, 1-kestose; 6K, 6-kestose.

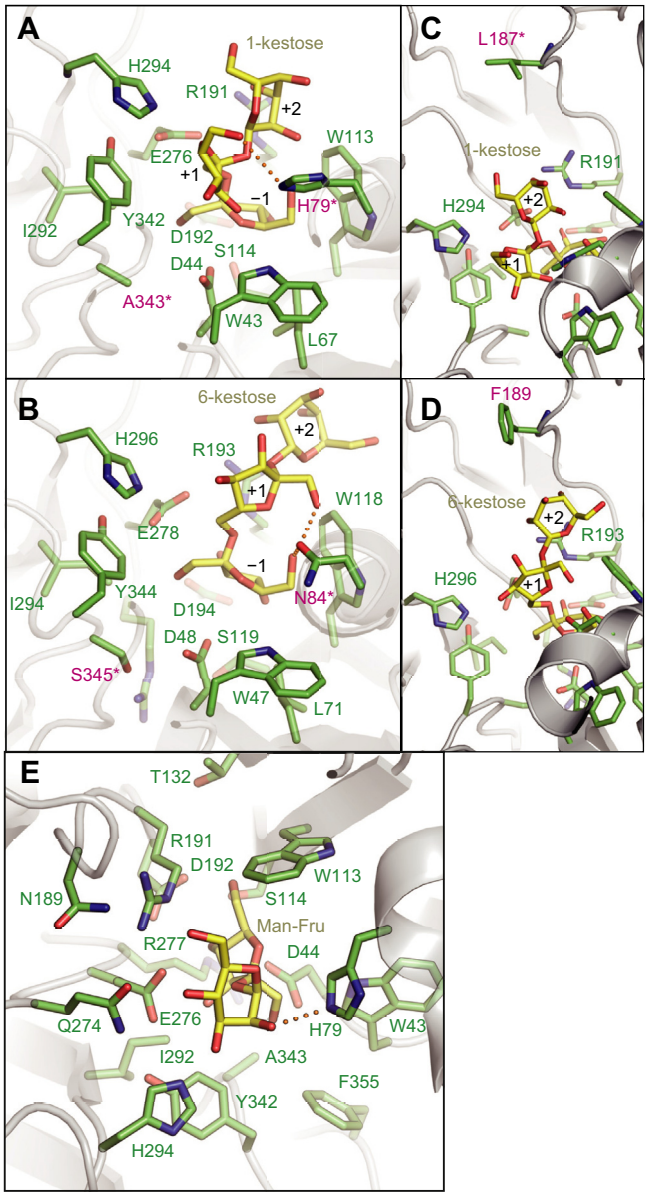

Figure 4. Structural models of FF*Zm* and LS*Zm* with ligands of 1-kestose (*A*, *C*), 6-kestose (*B*, *D*), and Fru-Man (*E*). *A* and *B*, catalytic pocket structures of FF*Zm* (*A*) and LS*Zm* (*B*) with 1-kestose and 6-kestose, respectively. Predicted hydrogen bonds are represented by orange dashed line between the mutation-candidate residues and ligands. *C* and *D*, structures around Leu187^{FFZm} and 1-kestose (*C*) as well as Phe189^{LSZm} and 6-kestose (*D*). In panel *A*–*D*, amino acid residues with stick-model are present within 3.5 Å from each ligand. Amino acid residues for mutagenesis are indicated with an asterisk (*A*–*C*). *E*, structural models of FF*Zm* with Fru-Man. Amino acid residues within 4.0 Å from Fru-Man are depicted as *sticks*. Predicted hydrogen bond is also shown by *orange dashed line* between His79FF and 2-OH of mannosyl residue. For all panels, Modeller constructed model structures of FF*Zm* and LS*Zm*. Autodock Vina docked 1-kestose or Fru-Man to FF*Zm* as well as 6-kestose, 1-kestose, or Fru-Man to LS*Zm*.

the neokestose production was detected at H79N-FF*Zm* and A343S-FF*Zm* but was hardly observed in the H79N/A343S-FF*Zm*. A little amount of tetrasaccharide nystose was produced by H79N-FF*Zm*, but H79N/A343S-FF*Zm* did not.

These results indicated that His79^{FFZm} and Ala343^{FFZm} are involved in the regioselectivity of 1-TF of FF*Zm*. The double mutation using two LS*Zm*-type residues enables FF*Zm* to synthesize the 6-kestose. However, FF*Zm* variants, gaining the 6-TF ability similarly to LS*Zm*, do not efficiently generate long LVOs with high DPs and levan, as compared with the parent LS*Zm*, which can do (inset of Fig. 3*B*). Only the H79N/A343S-FF*Zm* can produce an exceedingly small amount of LVOs having DP7 or less (Fig. 6, described below).

Functions of mutated residues

Our mutational study reveals that the position at the His79^{FF} or at its equivalent Asn84^{LS} is involved in the regioselectivity for 1-TF of FF*Zm* or 6-TF of LS*Zm*, respectively. The model structures suggest that His79^{FFZm} and Asn84^{LSZm} form hydrogen bonds with the hydroxy groups of 1-kestose and 6-kestose, respectively (Fig. 4, *A* and *B*). Introduction of Asn at His79^{FFZm} allows the formation of the hydrogen bond suitable to produce 6-kestose. Contrarily, the replacement of Asn84^{LSZm} with His may enable to form the hydrogen bonds suitable for 1-kestose synthesis. Besides, Ala343^{FF} and Ser345^{LS} are also concerned in the regioselectivity of the transfructosylation, although their mutations affect modestly rather than those of His79^{FFZm} and Asn84^{LSZm}. It is hard to interpret how the Ala343^{FFZm} and Ser345^{LSZm} contribute to the selectivity because these residues cannot contact directly to the substrate or product from each position, that is, the inner part of catalytic pocket (Fig. 4, *A* and *B*). However, the mutations of Ala343^{FFZm} and Ser345^{LSZm} are able to alter the orientation of the side chains of adjacent amino acid residues, such as Tyr342^{FFZm} and Tyr344^{LSZm}, both of which lie at the +1 subsite. The alteration could modify the architecture of the +1 subsite, influencing the transfructosylation process containing regioselectivity.

The relevant positions are conserved as a pair of His and Ala or that of Asn and Ser in the UniRef50_F8DT27 cluster, to which FF*Zm* and LS*Zm* belong. The enzymes having the former pair are predicted to be FF, whereas other enzymes having the latter pair are LS. On the other hand, the relationship between the residue pair and the regioselectivity of transfructosylation is found to be not necessarily conserved in GH68. Numerous GH68 enzymes derived from Gram-negative bacteria have a pair of His and Ser, although atypical for FF*Zm* or LS*Zm*. It has been demonstrated that LS*Gd* and LS*Ea* with this pair produce 1-kestose and nystose in addition to levan (18, 20). Their reaction specificities are more similar to that of LS*Zm* having a pair of Asn and Ser than that of A343S^{FFZm} and N79H^{LSZm}, which possess a pair of His and Ser. A further atypical example is the LS from Gram-positive bacteria, such as LS*Bc* and *Bacillus megaterium* LS (LS*Bm*), which have Ser at the second position of pair residue, corresponding to Ala343^{FFZm} and Ser345^{LSZm}; however, neither LS*Bc* nor LS*Bm* has a comparable residue, because the loop, carrying the relevant residue, is short. These LSs have been reported to possess another structural factor involved in the regioselectivity, at which a substitution of Arg370^{LSBm} with Gln is observed to increase 1-kestose synthesis (34). These concrete examples suggest a diversity of the relationship between structure and specificity in GH68 enzymes.

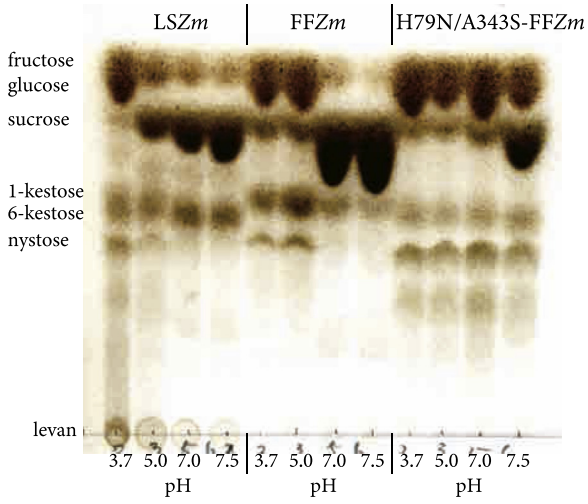

Figure 5. TLC analysis of levan- and long LVO-formation by LS*Zm*, FF*Zm* and H79N/A343S-FF*Zm*. LS*Zm*, FF*Zm* and H79N/A343S-FF*Zm* were incubated with 1 M sucrose at pH 3.7, 5.0, 7.0, and 7.5. Reaction was performed at 37 °C for 24 h. A spot of levan and quite long LVO appears at original position due to their large DP.

Levan synthesis using FFZm mutants

While H79N/A343S-FF*Zm* can catalyze the 6-TF, this mutant is devoid of synthesizing levan-type polysaccharides (Fig. 3*D*). Goldman *et al.* demonstrated that the levan production of *Z. mobilis* LS from ATCC10988 was related to its protein form depending on the pH (27). Below pH 6.0, the enzyme formed the well-ordered microfibril-shaped structure and synthesized levan, allowing us to conduct the levan-generation at pH 3.7–7.5 using H79N/A343S-FF*Zm* together with LS*Zm* and FF*Zm* as controls (LS*Zm* as a positive control and FF*Zm* as a negative control). The analysis using thin-layer chromatography (TLC) showed that LS*Zm* produced levan and/or long LVOs at any pH, although such saccharides were not generated by FF*Zm* and H79N/A343S-FF*Zm* (Fig. 5). As shown by Goldman *et al.* (27), the levan synthesis of LS*Zm* is more efficient at a lower pH. The pH is unrelated to the H79N/A343S-FF*Zm*-associated levan formation, suggesting that this mutant possesses further essential factor(s).

The structural factors of LS*Bspp* for levan synthesis are well-studied (16, 34–37), mentioning that Tyr247^{LSBm}, Asn252^{LSBm}, Asp257^{LSBm}, Arg370^{LSBm}, and Lys373^{LSBm} (the residue numbers are of LS*Bm*) were responsible for levan generation. Among them, the position of Asn252^{LSBm} is found to be divergent at FF*Zm* and LS*Zm*. Other residues are conserved in FF*Zm* (and also LS*Zm*), probably without being involved in the elongation by 6-TF. Asn252^{LSBm}, locating at a surface loop to connect blades II and III of 5-bladed β-propeller, is conserved in LS*Bspp*, although it varies in other GH68 enzymes. In FF*Zm* and LS*Zm*, Leu187^{FFZm} and Phe189^{LSZm} are equivalent to Asn252^{LSBm} (Fig. 4, *C* and *D*). In addition, Phe189^{LSZm} seems situated at a possible subsite far from −1 and +1 subsite of LS*Zm*, based on its model structure. We thus anticipated that the divergence of Leu187^{FFZm} and Phe189^{LSZm} is concerned with the ability (LS*Zm*) or inability (FF*Zm*) of levan synthesis.

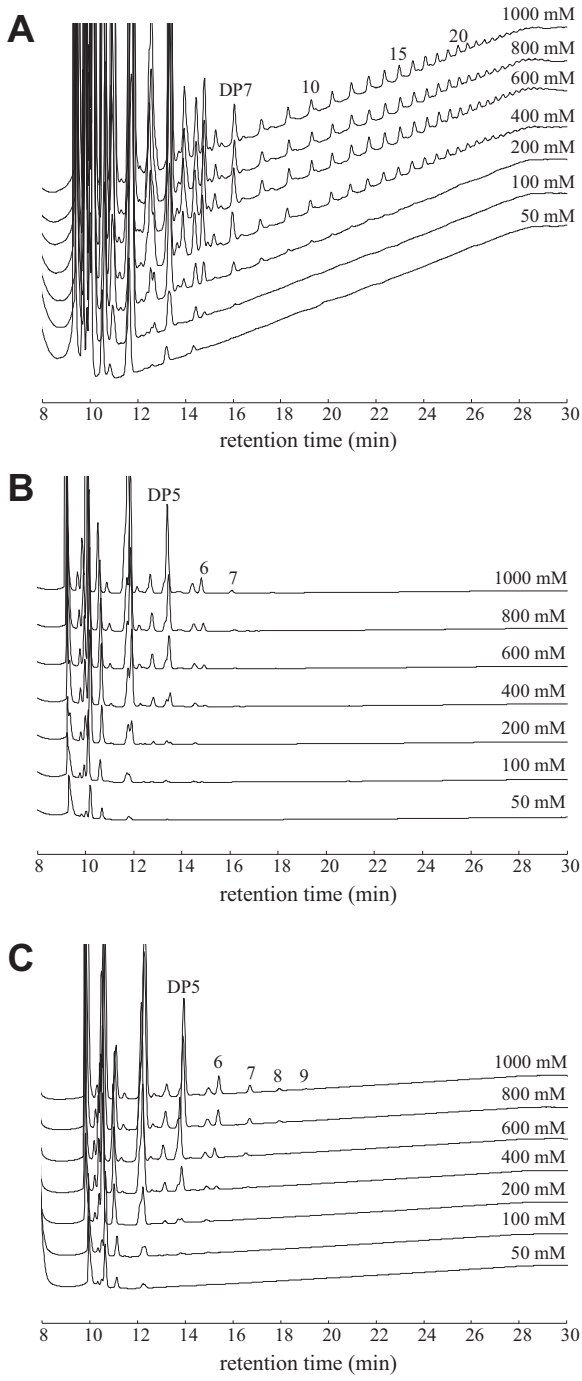

Figure 6. Long LVO formation of H79N/L187F/A343S-FF*Zm*. *A*, LS*Zm*; (*B*) H79N/A343S-FF*Zm*; (*C*) H79N/L187F/A343S-FF*Zm*. LS*Zm* (*A*), H79N/A343S-FF*Zm* (*B*), and H79N/L187F/A343S-FF*Zm* (*C*) were incubated with various [sucrose] (50, 100, 200, 400, 600, 800, and 1000 mM) in 30 mM sodium acetate buffer (pH 5.0) containing 0.01% Triton X-100 at 37 °C for 24 h, followed by analysis using HPAEC-PAD. Numbers on peaks are DP of their saccharides.

H79N/L187F/A343S-FF*Zm* was generated using H79N/A343S-FF*Zm* as a parent enzyme to exam its ability in association with the levan synthesis by the substitution of Leu187^{FFZm} with Phe. The specific activity of H79N/L187F/A343S-FF*Zm* was 350 U mg^{-1}, corresponding to 22% of FF*Zm* and 128% of H79N/A343S-FF*Zm* (Table 1). This triple mutant

Table 3
Fru-Man synthesis of FF*Zm*, LS*Zm*, and their variants

Enzyme	$\nu_{\text{Fru-Man}}$ $[E]_0^{-1}$ (s^{-1})	Yield (mM)
FF*Zm*		
Wild type	105	60
H79N-FF*Zm*	14	18
A343S-FF*Zm*	7.2	29
H79N/A343S-FF*Zm*	2.7	16
LS*Zm*		
Wild type	3.6	20
N84H-LS*Zm*	8.8	24
S345A-LS*Zm*	6.1	19
N84H/S345A-LS*Zm*	26	30

showed similarity in optimum pH and pH-stability, while heat stability was slightly decreased. The initial reaction velocities (Table 2) indicated that the ν_{Glc} (meaning a total reaction velocity), $\nu_{\text{6-Kes}}$, $\nu_{\text{1-Kes}}$, as well as transfructosylation ratio increased compared with those of H79N/A343S-FF*Zm*. The $[\nu_{\text{6-kestose}}/(\nu_{\text{1-kestose}} + \nu_{\text{6-kestose}})]$ value was almost the same as that of H79N/A343S-FF*Zm*, meaning that triple mutant maintains 6-GT regioselectivity.

Figure 6 shows the transfructosylation products of H79N/L187F/A343S-FF*Zm* from 0.05 to 1.0 M sucrose at 24 h with H79N/A343S-FF*Zm* and LS*Zm* as controls. Wild-type LS*Zm* appreciably synthesized long LVOs with DP20 or more from 400 mM sucrose or more (Fig. 6*A*), under which conditions we observed a trace amount of long LVOs from 200 mM sucrose. Almost no product above DP10 was formed from less than 100 mM sucrose. In Figure 5, a couple of unknown oligosaccharide spots under the position of the standard tetrasaccharide nystose were exhibited by H79N/A343S-FF*Zm* with a more significant intensity in comparison with that of wild-type FF*Zm* observed at any pH, although the TLC analysis could not clarify their DPs. The main oligosaccharide had DP5, and those of others were up to DP7 (Fig. 6*B*). H79N/L187F/A343S-FF*Zm* did not form any exceedingly long LVOs in contrast with LS*Zm* (Fig. 6*C*). Instead, this triple mutant formed the oligosaccharides of up to DP9. Mutation of Leu187$^{\text{FF}Zm}$ to Phe resulted in a slight increase in DP compared with that of its parent H79N/A343S-FF*Zm*. The Leu187$^{\text{FF}Zm}$ and Phe189$^{\text{LS}Zm}$ corresponding to Asn252$^{\text{LS}Bm}$ are subtly involved in elongating fructosyl units. Wild-type LS*Zm* might have further unknown structural factor(s) for the elongation.

Transfructosylation with mannose as accepter

GH68 enzymes have been used for the production of sucrose analogs (disaccharides) and glycosyl[glycosyl]$_n$sucrose ($n \geq 0$; DP 3 and over) by their transfructosylation (28, 38, 39). Although most of these saccharides can be produced in high yields using LS*Bc*, the sucrose analog Fru-Man has been quite difficult to be synthesized (0.3% maximum yield) (28). We thus explored the possible involvement of FF*Zm*, LS*Zm*, and their variants in the formation of Fru-Man. It was found that each enzyme was able to generate Fru-Man, as well as that the FF*Zm* was the most useful among all the used enzymes, as mentioned below. Oligosaccharides that were further synthesized included nystose, 1-kestose, and two kinds of unknown disaccharides, the structures of which were almost identified with associated results appearing elsewhere. Using 0.5 M sucrose as a donor substrate and 1.0 M mannose as an acceptor substrate, we measured the initial velocity of Fru-Man synthesis ($\nu_{\text{Fru-Man}}$ $[E]_0^{-1}$; abbreviated as ν_{FM}) and the yield of Fru-Man at 24 h of late reaction (Table 3). FF*Zm* shows by far the highest ν_{FM}, 105 s^{-1}, whereas the ν_{FM} values of FF*Zm* mutants are 2.6–13% of FF*Zm* ν_{FM}, and the ν_{FM} values of LS*Zm* and its mutants (except for N84H/S345A-LS*Zm* having 25%) are 3.4–8.4% of FF*Zm* ν_{FM}. While LS*Zm* variants carry low ν_{FM} values, these are 1.7–7.2-times larger than wild-type LS*Zm* does. Besides, the concentration of Fru-Man produced at 24 h became 60 mM (Table 3), which means that 12% of sucrose is converted to be Fru-Man. This is the greatest yield among the enzymes tested, as other enzymes generate 27–50% compared with that of FF*Zm*.

Seibel *et al.* (28) proposed that the LS*Bc*-associated small yield of Fru-Man was in association with the reduction of catalytic efficiency due to the deprivation of the hydrogen bond between general acid/base catalyst (Glu342$^{\text{LS}Bc}$) and axial 2-OH of mannose. Since the spatial position of the general acid/base would be conserved in the GH68 members, the Fru-Man-generating FF*Zm* also forms this hydrogen bond, suggesting that LS*Bc* has unknown factor(s) to reduce Fru-Man yield. It is assumed that a reason why FF*Zm* can synthesize Fru-Man is due to the His79$^{\text{FF}Zm}$ to stabilize the Fru-Man synthetic reaction. The model structure of FF*Zm* docking Fru-Man appears to depict the interaction between His79$^{\text{FF}Zm}$ and the axial 2-OH of mannose (Fig. 4*E*), indicative of the possible significance of His79$^{\text{FF}Zm}$. The fact that Fru-Man syntheses are decreased by both H79N-FF*Zm* and H79N/A343S-FF*Zm*, in which His79$^{\text{FF}Zm}$ is replaced, whereas the yields are inversely increased by N84H-LS*Zm* and N84H/S345A-LS*Zm*, which newly acquire His79$^{\text{FF}Zm}$, supporting the proposed interpretation. As previously mentioned, LS*Bspp* does not have a residue corresponding to His79$^{\text{FF}Zm}$. This absence might be one reason for LS*Bc* to accept a small amount of mannose into its catalytic site. On the other hand, it is difficult to explain that A343S-FF*Zm* and S345A-LS*Zm* alternate the Fru-Man production (ν_{FM} and yield) in comparison with their wild types, because, as mentioned earlier, Ala343$^{\text{FF}Zm}$ and Ser345$^{\text{LS}Zm}$ do not directly contact with the substrate sucrose. Similarly to the changes in regioselectivity, the orientation of the adjacent Tyr residue, Tyr342$^{\text{FF}Zm}$ and Tyr344$^{\text{LS}Zm}$, may be responsible for the changes in Fru-Man synthesis.

Conclusion

We have truly realized how important the analysis of the paralogous relationship in the field of protein engineering through the present study. Generally, one of the two paralogous proteins is thought to evolve independently and uniquely because its gene has undergone

relatively less restricted indels and substitutions. Therefore, the study of paralogous proteins is equivalent to the analysis of the results of protein engineering in nature and often provides important insights into the structure–function relationship of a protein. Based on this background, we have identified His79^{FFZm} and Ala343^{FFZm} and their respectively corresponding Asn84^{LSZm} and Ser345^{LSZm} as the amino acid residues associated with the regioselectivity in transfructosylation. We also demonstrated that Phe189^{LSZm} is fairly involved in the elongation of the fructosyl residues in levan synthesis by analyzing an H79N/L187F/A343S-FF*Zm*. In some cases, a gene that has undergone the less restricted mutations can often lose its function and become a pseudogene. However, in FFZm and LSZm, both enzymes were present with sufficient specific activity. This may be because *Z. mobilis* is only able to utilize sucrose as a disaccharide, and the enzymes engaged in sucrose degradation may be able to have evolved without losing their function.

Experimental procedures

Gene cloning, production, and purification of FFZm and LSZm

Genes of ZZ6_0874 and ZZ6_0875 locus_tags, respectively encoding FF*Zm* and LS*Zm*, were amplified from the chromosomal DNA of *Z. mobilis* NBRC 13756 (ATCC 29191) by PCR using primers: for ZZ6_0874, [5′-CGCGAGCTCTTTAATTTTAATGC-3′ (sense; *Sac*I-site underlined) and 5′-GAGTCTAGATTATTTGCGACGAT-3′ (antisense; *Xba*I-site underlined)]; and for ZZ6_0875, [5′-TCAACATGTTGAAATAAAGCAGGCATTGC-3′ (sense; *Pci*I-site underlined) and 5′-AAACTCGAGTTTATTCAATAAGACAGGGCTG-3′ (antisense; *Xho*I-site underlined)]. The primers were designed based on the published whole genome sequence of *Z. mobilis* ATCC 29191 (accession number, CP003704.1). After amplification using PrimeSTAR MAX DNA polymerase (Takara Bio), a PCR product for FF*Zm* was restricted with *Sac*I and *Xba*I and cloned into appropriately digested pColdI DNA (Takara Bio). The completed plasmid DNA was named pCold-FF*Zm*. A PCR product for LS*Zm* was digested with *Pci*I and *Xho*I and ligated to pET23 days (+) DNA (Novagen-Merck Millipore) predigested with *Nco*I and *Xho*I. The resulting plasmid DNA was called pET23-LSZm.

For the expression of FF*Zm*, *Escherichia coli* BL21(DE3) cells harboring pCold-FFZm were cultured in Luria–Bertani medium (10 g L^{-1} Bacto tryptone, 5 g L^{-1} Bacto yeast extract, and 5 g L^{-1} NaCl) supplemented with 0.1 g L^{-1} ampicillin at 37 °C until reaching mid-exponential phase (OD600 = ∼0.4), followed by cooling on ice. To culture the 2500^{-1} volume of 0.5 M isopropyl β-thiogalactoside was added, and cells were grown in a shaking incubator at 15 °C for 24 h. For the expression of LS*Zm*, *E. coli* BL21(DE3) cells harboring pET23-LSZm were cultured by shaking in an auto-inducing medium (40) [10 g L^{-1} Bacto tryptone, 5 g L^{-1} Bacto yeast extract, 50 mM Na_2HPO_4, 50 mM KH_2PO_4, 25 mM $(NH_4)_2SO_4$, 2 mM $MgSO_4$, 5 g L^{-1} glycerol, 5 g L^{-1} glucose, and 2 g L^{-1} lactose] supplemented with 0.1 g L^{-1} ampicillin at 30 °C for 24 h. The cells bearing FF*Zm* or LS*Zm* were harvested by centrifugation (5000*g*, 5 min, 4 °C), resuspended in 20 mM sodium phosphate, 300 mM NaCl, pH 8.0 (buffer A), and disrupted by sonication. The supernatant was obtained by centrifugation (20,000*g*, 20 min, 4 °C).

Recombinant proteins were purified from the above supernatant, loaded onto a Ni^{2+}-chelating Sepharose Fast Flow column (GE healthcare), which was prepared according to the instructions of manufacturer and pre-equilibrated with buffer A. After washing the column with buffer A containing 20 mM imidazole, the absorbed proteins were quickly eluted with 300 mM imidazole in buffer A, and then the pH of effluent immediately changed to pH 6.0 for FF*Zm* or to pH 5.0 for LS*Zm*. Active fractions were passed through a Bio-Gel P-6 (Bio-Rad) column pre-equilibrated with 20 mM sodium phosphate (pH 6.0) for FF*Zm* or with 20 mM sodium acetate (pH 5.0) for LS*Zm*. The obtained fractions were pooled and concentrated using a 30 kDa MWCO Vivaspin 20 (Sartorius AG). The concentration of purified enzyme ([enzyme]) was estimated by amino acid analysis of protein hydrolysate (6 M HCl, 110 °C, 24 h) using an Amino Acid Analyzer L-8900 (Hitachi High-Tech) equipped with a ninhydrin-detection system.

Construction of model 3D protein structures

Model 3D structures were prepared using the Modeller (41), Dock prep (31), and Autodock Vina (33) functions of UCSF Chimera version 1.14 (http://www.rbvi.ucsf.edu/chimera) (42). A template structure (PDB identifier, 4D47) was selected by Sequence Navigator server (https://pdbj.org/seqNavi). All model building was done with the default settings of the software. The GHECOM 1.0 server (https://pdbj.org/ghecom/) (43, 44) was used to detect the cavity in the docking simulation. Figures showing 3D structures were prepared using open-source PyMol (The PyMOL Molecular Graphic System version 2.4, Schrödinger, LLC). Sequence alignments were generated with T-coffee Expresso (http://tcoffee.crg.cat/apps/tcoffee/do:expresso) (45) or PROMALS3D (http://prodata.swmed.edu/promals3d/promals3d.php) (46).

Site-directed mutagenesis

Point mutations were introduced using the PrimeSTAR mutagenesis basal kit (Takara Bio). The oligonucleotides used for each mutation were as follows: for H79N-FF*Zm*, [5′-GATCGC**AAT**TCTCATGCCCGCATCGGC-3′ (sense; substituted codon in boldface) and 5′-ATGAGA**ATT**GCGATCATTCCACGGAAT-3′ (antisense)]; for A343S-FF*Zm*, [5′-GCCTAT**TCC**CATTACATCATGAATAAT-3′ (sense) and 5′-GTAATG**GGA**ATAGGCTTCGGTCGGCTG-3′ (antisense)]; for N84H-LS*Zm*, [5′-AATCGC**CAT**GATGGCGCCAGAATTGGT-3′ (sense) and 5′- GCCATC**ATG**GCGATTATGCCAACCATA-3′ (antisense)]; for S345A-LS*Zm*, [5′-GCTTAT**GCT**CATTATGTAATGACAAAT-3′ (sense) and 5′-ATAATG**AGC**ATAAGCCTGATAAGGCTG-3′ (antisense)]; for L187F-FF*Zm*, [5′-AATAAT**TTC**TGGAATTTCCGTGATCCT-3′ (sense) and 5′-ATTCCA**GAA**ATTATT

TTCTGCATAATT-3′ (antisense)]. The mutated enzymes were purified by the aforementioned procedures.

Enzyme assay and characterization

Enzyme activity was measured at 35 °C in a standard reaction mixture consisting of 50 mM sucrose (Nacalai Tesque), 30 mM sodium acetate buffer (pH 5.0), 0.01% Triton X-100, and appropriately diluted enzyme solution. Reaction was terminated by heating at 100 °C for 3 min. After adjusting pH to 7.0 by adding the double amount of 2 M Tris-HCl (pH 7.0), the concentration of liberated glucose in the reaction mixture was measured by a Glucose CII Test Wako (FUJIFILM Wako Pure Chemical). One unit of enzyme activity (U) was defined as the amount of enzyme that catalyzed the consumption of 1 μmol sucrose per minute under the above standard conditions.

pH-Dependent reaction velocities for identifying optimal pHs of FF*Zm*, LS*Zm*, and their variants were measured at 50 mM sucrose in the McIlvaine buffer (pH 3.9–7.0) containing 0.01% Triton X-100 at 35 °C. The [enzyme] used was specified for FF*Zm* (2.1 nM), LS*Zm* (2.0 nM), H79N-FF*Zm* (4.8 nM), A343S-FF*Zm* (4.0 nM), H79N/A343S-FF*Zm* (19 nM), H79N/L187F/A343S-FF*Zm* (4.2 nM), N84H-LS*Zm* (5.3 nM), S345A-LS*Zm* (0.34 nM), and N84H/S345A-LS*Zm* (2.6 nM). pH-Stable region was evaluated as follows: the enzyme (FF*Zm* [11 nM], LS*Zm* [10 nM], H79N-FF*Zm* [29 nM], A343S-FF*Zm* [25 nM], H79N/A343S-FF*Zm* [46 nM], H79N/L187F/A343S-FF*Zm* [52 nM], N84H-LS*Zm* [27 nM], S345A-LS*Zm* [9.0 nM], or N84H/S345A-LS*Zm* [13 nM]) was incubated with McIlvaine buffer (pH 2.7–7.0) for 24 h at 4 °C, and then the residual activity was determined at pH 5.0 according to the standard procedure described previously. To estimate the thermal stability of the enzymes, we incubated the enzyme (FF*Zm* [11 nM], LS*Zm* [10 nM], H79N-FF*Zm* [36 nM], A343S-FF*Zm* [12 nM], H79N/A343S-FF*Zm* [28 nM], H79N/L187F/A343S-FF*Zm* [32 nM], N84H-LS*Zm* [16 nM], S345A-LS*Zm* [5.1 nM], or N84H/S345A-LS*Zm* [7.8 nM]) containing 33 mM sodium acetate buffer (pH 5.0) and 0.01% Triton X-100 at 30–70 °C for 15 min, followed by measurement of the residual activity under the standard conditions described above.

HPAEC-PAD analysis

HPAEC-PAD was performed with a Dionex ICS-3000 system (Dionex/Thermo Fisher Scientific) using an analytical column (CarboPac PA1, 4 mm I.D. × 250 mm; Dionex/Thermo Fisher Scientific) and a flow rate of 0.8 ml min^{-1}. The eluent system comprised MilliQ water (a), 0.8 M NaOH prepared from super special grade 50% NaOH solution (FUJIFILM Wako Pure Chemical Co) (b), and 1.0 M sodium acetate (c), in which two procedures were used, namely method A and method B, as described below. In the method A, the products were separated by the elution system comprising the first linear gradient from 97.2:2.8:0 (% a:b:c) to 83.8:16.2:0 (% a:b:c) for 10 min and the second linear gradient from 83.8:16.2:0 (% a:b:c) to 65.9:24.1:10 (% a:b:c) for 6 min, followed by isocratic elution at 65.9:24.1:10 (% a:b:c) over 7 min. In the method B, the products were separated by a linear gradient from 87.5:12.5:0 (% a:b:c) to 51.5:12.5:36 (% a:b:c) from for 25 min, followed by isocratic elution at 51.5:12.5:36 (% a:b:c) over 5 min. Chromatograms were evaluated with Chromeleon software (Dionex/Thermo Fisher Scientific). The concentration of glucose, fructose, 1-kestose, 6-kestose, or neokestose was calculated using a calibration curve prepared based on the ration between chromatographic peak area of sorbitol as an internal standard and that of concentration-known saccharide standard. Neokestose was the kind gift from Prof Onodera S (Rakuno Gakuen University, Ebetsu, Japan).

Initial transfructosylation

For the measurement of v_{Glc}, v_{Fru}, $v_{1\text{-}Kes}$, and $v_{6\text{-}Kes}$, the reaction was done by incubating FF*Zm* (4.6 nM) or LS*Zm* (7.3 nM) with sucrose (0.025, 0.05, 0.1, 0.2, 0.3, 0.4, and 1.0 M) and 30 mM sodium acetate buffer (pH 5.0) containing 0.01% Triton X-100 at 35 °C for 10 min, followed by terminating reaction using heat treatment at 100 °C for 3 min. We also measured v_{Glc}, v_{Fru}, $v_{1\text{-}Kes}$, and $v_{6\text{-}Kes}$ against 1.0 M sucrose using FF*Zm*, LS*Zm*, and their variants ([enzyme], 30 to 800 nM) in the same way. The concentration of carbohydrates was determined by HPAEC-PAD using method A. For the measurement of $v_{Fru\text{-}Man}$, 0.5 M sucrose and 1.0 M mannose were used as substrates, and the used [enzyme] was 2.2 μM (FF*Zm*), 16 μM (LS*Zm*), 2.4 μM (H79N-FF*Zm*), 5.8 μM (A343S-FF*Zm*), 9.3 μM (H79N/A343S-FF*Zm*), 2.7 μM (N84H-LS*Zm*), 6.8 μM (S345A-LS*Zm*), or 2.6 μM (N84H/S345A-LS*Zm*). Other experimental conditions were the same as those described above.

Late transfructosylation at 1 h and 24 h

For the qualitative analysis of the products of the transfructosylation of FF*Zm*, LS*Zm*, and their variants using 1.0 M sucrose, the reaction was performed at 35 °C and pH 5.0 for up to 24 h in 30 mM sodium acetate buffer (pH 5.0). The [enzyme] was 0.03 μM (FF*Zm*), 0.34 μM (LS*Zm*), 0.13 μM (H79N-FF*Zm*), 1.3 μM (A343S-FF*Zm*), 0.64 μM (H79N/A343S-FF*Zm*), 0.44 μM (H79N/L187F/A343S-FF*Zm*), 0.38 μM (N84H-LS*Zm*), 0.24 μM (S345A-LS*Zm*), or 0.26 μM (N84H/S345A-LS*Zm*). At 1 and 24 h, a part of the reaction mixture was recovered, heated at 100 °C for 3 min to terminate the reaction, and diluted to 100^{-1} with 10 mM sorbitol of internal standard. The reaction products were analyzed by HPAEC-PAD. Resultant reaction samples at 1 h and 24 h were analyzed by methods A and B, respectively.

For investigating the changes in the long LVO production of LS*Zm*, H79N/A343S-FF*Zm* and H79N/L187F/A343S-FF*Zm*, we incubated each enzyme with different [sucrose] bearing 0.05, 0.1, 0.2, 0.4, 0.6, 0.8, or 1 M at 35 °C and pH 5.0 for 24 h in 40 mM sodium acetate buffer (pH 5.0), followed by heating at 100 °C for 3 min. The reaction mixture was diluted with sorbitol solution and analyzed by HPAEC-PAD using method B.

For the Fru-Man synthesis, the reaction of FF*Zm* (2.2 μM), LS*Zm* (16 μM), H79N-FF*Zm* (2.4 μM), A343S-FF*Zm* (5.8 μM), H79N/A343S-FF*Zm* (9.3 μM), N84H-LS*Zm* (2.7 μM), S345A-LS*Zm* (6.8 μM), or N84H/S345A-LS*Zm* (2.6 μM) was performed with 0.5 M sucrose and 1.0 M mannose at 35 °C and pH 5.0 for 24 h, and was subsequently terminated by heating at 100 °C for 3 min. A sample for HPAEC-PAD analysis using method A was prepared by 100^{-1}-dilution of reaction mixture with 10 mM sorbitol.

pH-Influence on production of long LVO and levan

For analyzing the synthesis of long LVO and levan at the different pHs, we incubated H79N/A343S-FF*Zm*, FF*Zm*, or LS*Zm* (5 U mL^{-1} for each enzyme) with 1.0 M sucrose in McIlvaine buffer (pH 3.7, 5.0, 7.0, and 7.5) for 24 h at 35 °C. After heat treatment at 100 °C for 3 min, the reaction mixture was appropriately diluted in deionized water and analyzed by TLC using a TLC-plate (0.25-mm layers of silica gel 60 F_{254}; Merck Millipore). The separation of carbohydrates was done using acetonitrile:water (75:25, v/v) as the developing solvent by three-times ascent, followed by visualization with spraying an α-naphthol/sulfuric acid solution (15% sulfuric acid in methanol containing 2.1 mM α-naphthol) and heating at 110 °C for 5 min.

Production of 6-kestose and Fru-Man

This research required the preparation of an appropriate amount of standard 6-kestose. For this, we did the 10 ml-level reaction of 37 U mL^{-1} H79N/A343S-FF*Zm* with 1.0 M sucrose at 35 °C and pH 5.0 for 2 h. Reaction solution was desalted by Amberlite MB-4 resin (Organo), and then concentrated to 2 ml under reduced pressure. The reaction products were separated by an HPLC system (Jasco) equipped with a refractive index monitor (Jasco RI-2031) with a Cosmosil Sugar-D column (10 mm I.D. × 250 mm; Nacalai Tesque). Separation was achieved using a mobile phase (acetonitrile:water, 80:20, v/v) with a flow rate of 3 ml min^{-1}. For Fru-Man synthesis, 1.25 M sucrose and 2.5 M mannose with 25 U mL^{-1} FF*Zm* in 10 ml of 40 mM sodium acetate buffer were incubated at 35 °C for 6 h. The reaction mixture was divided into three equal parts and was fractionated by gel filtration chromatography using Bio-Gel P-2 Gel (1.6 cm I.D. × 190 cm, Bio-Rad). Fractions containing Fru-Man were recovered and concentrated under reduced pressure. Reducing sugars were decomposed by the incubation with 2 M NaOH at 100 °C for 10 min. The reaction solution was neutralized by adding Amberlite IR120 H^+ form and decolorized by activated carbon. The resulting samples were again subjected to gel filtration chromatography and purified Fru-Man was obtained. The molecular masses of oligosaccharide products were confirmed by ESI-MS using a Thermo Scientific Exactive spectrometer (Thermo Fisher Scientific, Inc). ^{13}C-NMR (126 MHz) spectra were recorded on a Bruker AVANCE I (Bruker). The relative values of the chemical shifts for 6-kestose and Fru-Man were in agreement with those previously reported (47, 48). 6-Kestose: ^{13}C-NMR (126 MHz, D_2O) δ (ppm): 106.6 (C-2′, C-2″), 95.0 (C-1), 84.0 (C-5″), 83.1 (C-5′), 79.3 (C-3″), 79.0 (C-3′), 77.5 (C-4″), 77.2 (C-4′), 75.4 (C-3), 75.2 (C-5), 73.9 (C-2), 72.1 (C-4), 65.8 (C-6′), 65.4 (C-6″), 64.0 (C-1′), 63.1 (C-6), 62.6 (C-1″); MS: *m/z* calculated: 527.16 $[M+Na]^+$, 503.16 $[M - H]^-$; found 527.16, 503.16. Fru-Man: ^{13}C-NMR (126 MHz, D_2O) δ (ppm): 104.8 (C-2′), 94.4 (C-1), 82.2 (C-5′), 76.8 (C-3′), 74.7 (C-4′), 74.1 (C-2), 71.9 (C-3), 71.0 (C-5), 67.3 (C-4), 63.3 (C-6′), 61.8 (C-1′), 61.5 (C-6); MS: *m/z* calculated: 365.11$[M+Na]^+$, 341.11 $[M - H]^-$; found 365.11, 341.11.

Data availability

The authors indicate that all of the data is contained within the article.

Acknowledgments—We would like to thank Prof Onodera S (Rakuno Gakuen University) for kindly gifting us neokestose. We also thank the staff of the Instrumental Analysis Division of the Creative Research Institution at Hokkaido University for the conduction of amino acid analysis and mass spectrometry analysis, and the staff of the GC-MS & NMR Laboratory in the Research Faculty of Agriculture at Hokkaido University for NMR analysis.

Author contributions—M. O., T. T., and A. K. conceived and coordinated the study. M. O., R. S., M. T., A. K., J. S., and W. L. performed the experiments and analyzed data. M. O. and A. K. created the manuscript. M. O. and A. K. provided essential equipment and facilities. M. O. and R. S. contributed equally. All the authors reviewed the results and approved the final version of this article.

Funding and additional information—This work was partly supported by the Japan Society for the Promotion of Science KAKENHI Grant Nos. 26450114 and 17H03801.

Conflict of interest—The authors declare that they have no conflicts of interest with the contents of this article.

Abbreviations—The abbreviations used are: DP, degree of polymerization; *Ea*Lsc, levansucrase from *Erwinia amylovora*; FF, β-fructofuranosidase; FF*Zm*, *Zymomonas mobilis* FF; FOS, fructooligosaccharides; Fru-Man, β-D-fructofuranosyl α-D-mannopyranoside; GH, glycoside hydrolase family; HPAEC-PAD, high-performance anion-exchange chromatography with pulsed amperometric detection; INO, inulooligosaccharide; LS, levansucrase; LS*Bc*, *Bacillus subtilis* LS; LS*Bspp*, *Bacillus* spp. LS; LS*Bm*, *Bacillus megaterium* LS; LS*Ea*, *Erwinia amylovora* LS; LS*Gd*, *Gluconacetobacter diazotrophicus* LS; LS*Zm*, *Zymomonas mobilis* LS; LVO, levanooligosaccharide; TLC, thin-layer chromatography; ν_{FM}, $\nu_{Fru\text{-}Man}$ $[E]_0^{-1}$; ν_{Fru}, $\nu_{fructose}$ $[E]_0^{-1}$; ν_{Glc}, $\nu_{glucose}$ $[E]_0^{-1}$; $\nu_{1\text{-}Kes}$, $\nu_{1\text{-}kestose}$ $[E]_0^{-1}$; $\nu_{6\text{-}Kes}$, $\nu_{6\text{-}kestose}$ $[E]_0^{-1}$; 3D, three-dimensional structure; 1-TF, β-(2→1)-transfructosylation; 6-TF, β-(2→6)-transfructosylation.

References

1. Versluys, M., Kirtel, O., Öner, E. T., and Van den Ende, W. (2018) The fructan syndrome: Evolutionary aspects and common themes among plants and microbes. *Plant Cell Environ.* **41**, 16–38
2. Belorkar, S. A., and Gupta, A. K. (2016) Oligosaccharides: A boon from nature's desk. *AMB Express* **6**, 82

3. Tochio, T., Kadota, Y., Tanaka, T., and Koga, Y. (2018) 1-Kestose, the smallest fructooligosaccharide component, which efficiently stimulates *Faecalibacterium prausnitzii* as well as bifidobacteria in humans. *Foods* **7**, 9
4. Scholz-Ahrens, K. E., and Schrezenmeir, J. (2007) Inulin and oligofructose and mineral metabolism: The evidence from animal trials. *J. Nutr.* **137**, 2513S–2523S
5. Cairns, A. J., Nash, R., De Carvalho, M. A. M., and Sims, I. M. (1999) Characterization of the enzymatic polymerization of 2,6-linked fructan by leaf extracts from timothy grass (*Phleum pratense*). *New Phytol.* **142**, 79–91
6. Tamura, K., Kawakami, A., Sanada, Y., Tase, K., Komatsu, T., and Yoshida, M. (2009) Cloning and functional analysis of a fructosyltransferase cDNA for synthesis of highly polymerized levans in timothy (*Phleum pratense* L.). *J. Exp. Bot.* **60**, 893–905
7. Rodrigo-Frutos, D., Piedrabuena, D., Sanz-Aparicio, J., and Fernández-Lobato, M. (2019) Yeast cultures expressing the Ffase from *Schwanniomyces occidentalis*, a simple system to produce the potential prebiotic sugar 6-kestose. *Appl. Microbiol. Biotechnol.* **103**, 279–289
8. de Abreu, M., Alvaro-Benito, M., Sanz-Aparicio, J., Plou, F. J., Fernandez-Lobato, M., and Alcalde, M. (2013) Synthesis of 6-kestose using an efficient β-fructofuranosidase engineered by directed evolution. *Adv. Synth. Catal.* **355**, 1698–1702
9. Linde, D., Rodríguez-Colinas, B., Estévez, M., Poveda, A., Plou, F. J., and Fernández Lobato, M. (2012) Analysis of neofructooligosaccharides production mediated by the extracellular β-fructofuranosidase from *Xanthophyllomyces dendrorhous*. *Bioresour. Technol.* **109**, 123–130
10. Álvaro-Benito, M., A. Sainz-Polo, M., González-Pérez, D., González, B., Plou, F. J., Fernández-Lobato, M., and Sanz-Aparicio, J. (2012) Structural and kinetic insights reveal that the amino acid pair Gln-228/Asn-254 modulates the transfructosylating specificity of *Schwanniomyces occidentalis* β-fructofuranosidase, an enzyme that produces prebiotics. *J. Biol. Chem.* **287**, 19674–19686
11. Ueno, K., Onodera, S., Kawakami, A., Yoshida, M., and Shiomi, N. (2005) Molecular characterization and expression of a cDNA encoding fructan: fructan 6(G)-fructosyltransferase from asparagus (*Asparagus officinalis*). *New Phytol.* **165**, 813–824
12. Lasseur, B., Lothier, J., Djoumad, A., De Coninck, B., Smeekens, S., Van Laere, A., Morvan-Bertrand, A., Van den Ende, W., and Prud'homme, M.-P. (2006) Molecular and functional characterization of a cDNA encoding fructan:fructan 6G-fructosyltransferase (6G-FFT)/fructan:fructan 1-fructosyltransferase (1-FFT) from perennial ryegrass (*Lolium perenne* L.). *J. Exp. Bot.* **57**, 2719–2734
13. Cantarel, B. L., Coutinho, P. M., Rancurel, C., Bernard, T., Lombard, V., and Henrissat, B. (2009) The Carbohydrate-Active EnZymes database (CAZy): An expert resource for Glycogenomics. *Nucleic Acids Res.* **37**, D233–D238
14. Porras-Domínguez, J. R., Ávila-Fernández, Á., Miranda-Molina, A., Rodríguez-Alegría, M. E., and Munguía, A. L. (2015) *Bacillus subtilis* 168 levansucrase (SacB) activity affects average levan molecular weight. *Carbohydr. Polym.* **132**, 338–344
15. Raga-Carbajal, E., López-Munguía, A., Alvarez, L., and Olvera, C. (2018) Understanding the transfer reaction network behind the non-processive synthesis of low molecular weight levan catalyzed by *Bacillus subtilis* levansucrase. *Sci. Rep.* **8**, 15035
16. Homann, A., Biedendieck, R., Götze, S., Jahn, D., and Seibel, J. (2007) Insights into polymer versus oligosaccharide synthesis: Mutagenesis and mechanistic studies of a novel levansucrase from *Bacillus megaterium*. *Biochem. J.* **407**, 189–198
17. Ortiz-Soto, M. E., Porras-Domínguez, J. R., Seibel, J., and López-Munguía, A. (2019) A close look at the structural features and reaction conditions that modulate the synthesis of low and high molecular weight fructans by levansucrases. *Carbohydr. Polym.* **219**, 130–142
18. Hernandez, L., Arrieta, J., Menendez, J., Vazquez, R., Coego, A., Suarez, V., Selman, G., Petit-Glatron, M. F., and Chambert, R. (1995) Isolation and enzymic properties of levansucrase secreted by *Acetobacter diazotrophicus* SRT4, a bacterium associated with sugar cane. *Biochem. J.* **309**, 113–118
19. Martínez-Fleites, C., Ortíz-Lombardía, M., Pons, T., Tarbouriech, N., Taylor, E. J., Arrieta, J. G., Hernández, L., and Davies, G. J. (2005) Crystal structure of levansucrase from the Gram-negative bacterium *Gluconacetobacter diazotrophicus*. *Biochem. J.* **390**, 19–27
20. Caputi, L., Nepogodiev, S. A., Malnoy, M., Rejzek, M., Field, R. A., and Benini, S. (2013) Biomolecular characterization of the levansucrase of *Erwinia amylovora*, a promising biocatalyst for the synthesis of fructooligosaccharides. *J. Agric. Food Chem.* **61**, 12265–12273
21. Loehlin, D. W., and Carroll, S. B. (2016) Expression of tandem gene duplicates is often greater than twofold. *Proc. Natl. Acad. Sci. U. S. A.* **113**, 5988–5992
22. Kyono, K., Yanase, H., Tonomura, K., Kawasaki, H., and Sakai, T. (1995) Cloning and characterization of *Zymomonas mobilis* genes encoding extracellular levansucrase and invertase. *Biosci. Biotechnol. Biochem.* **59**, 289–293
23. Yanase, H., Iwata, M., Nakahigashi, R., Kita, K., Kato, N., and Tonomura, K. (1992) Purification, crystallization, and properties of the extracellular levansucrase from *Zymomonas mobilis*. *Biosci. Biotechnol. Biochem.* **56**, 1335–1337
24. Yanase, H., Iwata, M., Kita, K., Kato, N., and Tonomura, K. (1995) Purification, crystallization, and characterization of the extracellular invertase from *Zymomonas mobilis*. *J. Ferment. Bioeng.* **79**, 367–369
25. Yanase, H., Maeda, M., Hagiwara, E., Yagi, H., Taniguchi, K., and Okamoto, K. (2002) Identification of functionally important amino acid residues in *Zymomonas mobilis* levansucrase. *J. Biochem.* **132**, 565–572
26. Li, S., Yan, Y., Zhou, Z., Yu, H., Zhan, Y., Zhang, W., Chen, M., Lu, W., Ping, S., and Lin, M. (2011) Single amino acid residue changes in subsite-1 of levansucrase from *Zymomonas mobilis* 10232 strongly influence the enzyme activities and products. *Mol. Biol. Rep.* **38**, 2437–2443
27. Goldman, D., Lavid, N., Schwartz, A., Shoham, G., Danino, D., and Shoham, Y. (2008) Two active forms of *Zymomonas mobilis* levansucrase: An ordered microfibril structure of the enzyme promotes levan polymerization. *J. Biol. Chem.* **283**, 32209–32217
28. Seibel, J., Moraru, R., Götze, S., Buchholz, K., Na'amnieh, S., Pawlowski, A., and Hecht, H. J. (2006) Synthesis of sucrose analogues and the mechanism of action of *Bacillus subtilis* fructosyltransferase (levansucrase). *Carbohydr. Res.* **341**, 2335–2349
29. Brumer, H., Sims, P. F., and Sinnott, M. L. (1999) Lignocellulose degradation by *Phanerochaete chrysosporium*: Purification and characterization of the main α-galactosidase. *Biochem. J.* **339**, 43–53
30. Liao, J., Okuyama, M., Ishihara, K., Yamori, Y., Iki, S., Tagami, T., Mori, H., Chiba, S., and Kimura, A. (2016) Kinetic properties and substrate inhibition of α-galactosidase from *Aspergillus niger*. *Biosci. Biotechnol. Biochem.* **80**, 1747–1752
31. Dolinsky, T. J., Nielsen, J. E., McCammon, J. A., and Baker, N. A. (2004) PDB2PQR: An automated pipeline for the setup of Poisson-Boltzmann electrostatics calculations. *Nucleic Acids Res.* **32**, W665–W667
32. Wuerges, J., Caputi, L., Cianci, M., Boivin, S., Meijers, R., and Benini, S. (2015) The crystal structure of *Erwinia amylovora* levansucrase provides a snapshot of the products of sucrose hydrolysis trapped into the active site. *J. Struct. Biol.* **191**, 290–298
33. Trott, O., and Olson, A. J. (2010) Software news and update AutoDock Vina: Improving the speed and accuracy of docking with a new scoring function, efficient optimization, and multithreading. *J. Comput. Chem.* **31**, 455–461
34. Possiel, C., Ortiz-Soto, M. E., Ertl, J., Münch, A., Vogel, A., Schmiedel, R., and Seibel, J. (2019) Exploring the sequence variability of polymerization-involved residues in the production of levan- and inulin-type fructooligosaccharides with a levansucrase. *Sci. Rep.* **9**, 1–11
35. Ortiz-Soto, M. E., Rivera, M., Rudiño-Piñera, E., Olvera, C., and López-Munguía, A. (2008) Selected mutations in *Bacillus subtilis* levansucrase semi-conserved regions affecting its biochemical properties. *Protein Eng. Des. Sel* **21**, 589–595
36. Strube, C. P., Homann, A., Gamer, M., Jahn, D., Seibel, J., and Heinz, D. W. (2011) Polysaccharide synthesis of the levansucrase SacB from *Bacillus megaterium* is controlled by distinct surface motifs. *J. Biol. Chem.* **286**, 17593–17600

37. He, C., Yang, Y., Zhao, R., Qu, J., Jin, L., Lu, L., Xu, L., and Xiao, M. (2018) Rational designed mutagenesis of levansucrase from *Bacillus licheniformis* 8-37-0-1 for product specificity study. *Appl. Microbiol. Biotechnol.* **102**, 3217–3228
38. Wu, C., Zhang, T., Mu, W., Miao, M., and Jiang, B. (2015) Biosynthesis of lactosylfructoside by an intracellular levansucrase from *Bacillus methylotrophicus* SK 21.002. *Carbohydr. Res.* **401**, 122–126
39. Win, T. T., Isono, N., Kusnadi, Y., Watanabe, K., Obae, K., Ito, H., and Matsui, H. (2004) Enzymatic synthesis of two novel non-reducing oligosaccharides using transfructosylation activity with β-fructofuranosidase from *Arthrobacter globiformis*. *Biotechnol. Lett.* **26**, 499–503
40. Studier, F. W. (2005) Protein production by auto-induction in high density shaking cultures. *Protein Expr. Purif.* **41**, 207–234
41. Šali, A., and Blundell, T. L. (1993) Comparative protein modeling by satisfaction of spatial restraints. *J. Mol. Biol.* **234**, 779–815
42. Pettersen, E. F., Goddard, T. D., Huang, C. C., Couch, G. S., Greenblatt, D. M., Meng, E. C., and Ferrin, T. E. (2004) UCSF Chimera-A visualization system for exploratory research and analysis. *J. Comput. Chem.* **25**, 1605–1612
43. Kawabata, T., and Go, N. (2007) Detection of pockets on protein surfaces using small and large probe spheres to find putative ligand binding sites. *Proteins* **68**, 516–529
44. Kawabata, T. (2010) Detection of multiscale pockets on protein surfaces using mathematical morphology. *Proteins* **78**, 1195–1211
45. Notredame, C., Higgins, D. G., and Heringa, J. (2000) T-coffee: A novel method for fast and accurate multiple sequence alignment. *J. Mol. Biol.* **302**, 205–217
46. Pei, J., Kim, B.-H., and Grishin, N. V. (2008) PROMALS3D: A tool for multiple protein sequence and structure alignments. *Nucleic Acids Res.* **36**, 2295–2300
47. Liu, J., Waterhouse, A. L., and Chatterton, N. J. (1991) Proton and carbon chemical-shift assignments for 6-kestose and neokestose from two-dimensional n.m.r. measurements. *Carbohydr. Res.* **217**, 43–49
48. Seibel, J., Moraru, R., and Götze, S. (2005) Biocatalytic and chemical investigations in the synthesis of sucrose analogues. *Tetrahedron* **61**, 7081–7086